한국소음진동공학회 2001년도 춘계학술대회논문집, pp. 751~756

음향파를 이용한 두 평행류의 혼합 증대

○신성룡*, 장세명**, 이수갑***

Numerical Simulation of Mixing Control in Parallel Supersonic-Subsonic Jet Using Acoustic Waves

Seong-Ryong Shin, Se-Myong Chang and Soogab Lee

Abstract

An experimental model of the advanced mixing control in the parallel supersonic-subsonic mixing jet (M_1=1.78 and M_2=0.30) is numerically simulated. An oscillating wall boundary condition is used as the modeling of a wall cavity for mixing enhancement. The obtained pitot pressure distributions along cross sections at the developing region of the turbulent jets are validated from the good agreement with equivalent experimental data. The similarity solution of dimensional analysis also coincides with this numerical result at the self-similar region sufficiently far from the jet exit.

1. Introduction

The geometry and flow conditions of interest in this paper are directly related with the combustor of SCRamjet engine. This is expected to be one of the most effective hypersonic propulsion systems. Owing to the innately low shear-induced mixing of high Mach number, fully developed turbulent free-shear layers, provisions for ensuring enhanced mixing in flight are particularly important. Until now many techniques that provide turbulent and mixing augmentation have been suggested and they may be classified into two categories: the direct forcing method using a spark charge and the indirect control method using unstable flow fields [1, 2]. One of the useful ideas to activate the fuel-air mixture using indirect control method is the use of a cavity emitting acoustic waves in a flow field [3, 4]. Especially, the authors of Ref.[4] performed a preliminary experimental study on the mixing enhancement of a parallel supersonic-subsonic jet with the use of acoustic waves emitted from a wall-mounted cavity in the supersonic flow field.

A typical schematic diagram of a parallel supersonic-subsonic jet-mixing problem is shown in Fig.1. The subsonic flow (M_2<1) is injected into the uniform supersonic flow (M_1>1) through a parallel nozzle, retaining its speed before a length of X_c from the nozzle exit. However, the free turbulent shear layers (Mixing layers) beginning at the aft tip of nozzle expanding gradually close to a point (End of core). The triangular region surrounded by mixing layers consists of a 'Potential core', and the collision of two layers beyond the end of core will expand the mixing region. After the 'Developing region', the width (b) of jet boundary has a constant

* 서울대 기계항공공학부 박사과정
** 서울대 기계항공공학부 계약교수, 공학박사
*** 서울대 기계항공공학부 교수, 공학박사

growing rate and the profile of wake velocity turns to a similarity solution along the jet axis: therefore, we call the fully developed region 'Self-preserving flow'.

In this paper, we reproduce the experiment of Ref. [4] with a numerical simulation solving Navier-Stokes equations. The cavity at the wall is just simplified to a sinusoidal oscillation of wall pressure with a primary. That is, the supersonic cavity acoustics is modeled into a 'vibrating-wall boundary condition'.

2. Methodology

2.1 Definition of the Present Problem

As shown in Fig.2, the computational domain consists of a block (120 mm x 40 mm), which is equivalent to the experimental setup of Ref.[4]. An oscillating region ON (a rectangular cavity in Ref. [4]) of 10 mm length is installed along the upper wall with a variable distance X_p from the normal projection point of nozzle exit. The free stream Mach number of supersonic base flow is M_1=1.78, and the subsonic flow M_2=0.30 is injected through a rectangular nozzle (3 mm inner gap and 0.5 mm thickness) in a two-dimensional manner. Total temperature is the same as the ambient temperature. The flow condition of a non-disturbed (without wall vibration) is listed as the following: u_1=473 m/s, u_2=100 m/s, ρ_1=2.0 kg/m^3, ρ_2=1.24 kg/m^3, and p_1=p_2=1.01310^5 N/m^2 where the subscript 1 and 2 mean the base and injected flows, respectively.

Then the wall pressure at the segment ON in Fig. 2 varies in times:

$$p = p_1 + p_a \sin \omega t \qquad (1)$$

where p_a is an amplitude, and ω is an angular frequency.

2.2 Governing Equations

Two-dimensional Navier-Stokes equations for inviscid compressible flows are written in the following tensor form:

$$\frac{\partial \mathbf{U}}{\partial t} + \frac{\partial \mathbf{F}_j}{\partial x_j} = \frac{\partial \mathbf{G}_j}{\partial x_j} \qquad i, j = 1,2 \qquad (2)$$

where

$$\mathbf{U}=\begin{pmatrix} \rho \\ \rho u_i \\ E \end{pmatrix}, \quad \mathbf{F}_j=\begin{pmatrix} \rho u_j \\ \rho u_i u_j + p\delta_{ij} \\ u_j(E+p) \end{pmatrix}, \quad \mathbf{G}_j=\begin{pmatrix} 0 \\ \tau_{ij} \\ u_i\tau_{ij}+q_j \end{pmatrix},$$

and

$$E = \frac{p}{\gamma - 1} + \frac{1}{2}\rho\, u_j u_j \quad , \qquad T = \frac{p}{\rho R} \quad ,$$

$$\tau_{ij} = \mu\left(\frac{\partial u_i}{\partial x_j} + \frac{\partial u_j}{\partial x_i}\right) - \frac{2}{3}\mu\delta_{ij}\left(\frac{\partial u_i}{\partial x_i}\right) \quad ,$$

$$q_j = k\frac{\partial T}{\partial x_j} = \frac{\gamma}{\gamma - 1}\frac{\mu}{\mathrm{Pr}}\frac{\partial}{\partial x_j}\left(\frac{p}{\rho}\right) \quad ,$$

$$\mu = \mu_0\left(\frac{T}{T_0}\right)^{3/2}\frac{T_0 + S}{T + S}$$

The above system of partial differential equations is integrated with a finite-volume numerical technique described in Section 2.4.

2.3 Boundary Conditions

A special treatment is needed for the oscillating boundary condition(Fig.3). In the actual computation, we only replace the no-slip boundary condition into a new one at ON because the tip grid cells are commonly regarded as ghost points buried in the solid wall. Considering one-dimensional flow dynamics in the vertical direction of Fig.3, following equations are derived after some manipulations

$$v = 0 \qquad (3)$$

$$\rho = \frac{\rho_1}{2\gamma}\left\{\gamma - 1 + (\gamma + 1)\frac{p}{p_1}\right\} \qquad (4)$$

Eq. (1) and (3)-(4) are a complete set of Dirichlet boundary condition for the vibrating surface at ON in Fig 2.

2.4 Numerical Technique

Eq. (2) is integrated with finite-volume flux difference method based on Roe approximate Riemann solver that uses the square-root weight average based on densities of left and right cells to evaluate a numerical flux at the boundary of a given cell. The temporal integration is formulated in an explicit manner, and the time step is dependent on the eigenvalues and the size of grids. The high-order accuracy for space and time is obtained by employing MUSCL algorithm. Overall, the present numerical scheme reserves the second-order accuracy in both space and time: the validation can also be found in reference [5].

2.5 Turbulence Modeling

By nature, the present problem depicted in Fig. 1-2 contains a lot of turbulence. This system is a kind of hybrid between a *free wake* in M_1=1.78 that lies obviously in the compressible flow regime and a *jet* of M_2=0.30 that might be looked upon as incompressible flow. However, their interaction is highly nonlinear, including a free turbulence, and therefore a turbulence model should be used for the modification of Eq.(2): the eddy viscosity (μ_t) is added to the viscosity (μ) in Eq.(2), and the new viscosity considering the turbulent diffusion is

$$\bar{\mu} = \mu + \mu_t \qquad (5)$$

Clauser's free-wake model is widely known to fit for various planar turbulent jet problems [6]. We modified this model using Görtler's similarity analysis on free wakes [7]. In the Clauser-Görtler model, the turbulence viscosity is simply defined as

$$\mu_t = K\rho(u_1 - u)b\left(\frac{x}{X_{ref}}\right)^{1/2}, K = 0.016 \qquad (6)$$

where b is the jet width at a reference position (X_{ref}). Eq. (6) is an incomplete model because we must know reference values, but they are evaluated from the solution of Navier-Stokes equations without turbulence model. Recall that the free turbulence is blocked from the potential core in Fig. 1, and we can set a reference point near the end of core. In spite of turbulence coupling, the Prandtl number is also fixed to 0.71 for this adverse-pressure jet problem, which is observed in experiment [8]. Eq. (6) includes no compressibility effect, but the present numerical result shows a good agreement with the experiment of Ref. [4] (later see Fig. 8a-d).

2.6 On the Nyquist Frequency

In the propagation of acoustic waves, common Navier-Stokes codes of second-order accuracy in Section 2.4 do not satisfy the dispersion relation. Therefore, only lower frequency than the Nyquist value can be transmitted without loss. The Nyquist frequency is theoretically evaluated to include more than two point values per period in the digitizing of a sinusoidal wave.

$$\nu_{Nyquist} = \frac{c}{2\Delta x} \qquad (7)$$

where Δx is the maximum grid size. However, as commented in Ref. [9], the dispersion-free acoustic propagation requires about 10 to 20 data points, and therefore the Nyquist frequency is 1/10 to 1/20 of the theoretical one of Eq. (7).

3. Results and Discussion

The authors of Ref. [4] used a L/D = 2 cavity to generate acoustic waves where L is the width and D

is the depth of cavity. To fix the noise source (p_a and ω in Eq. (1)), we must know the acoustic physics of experimental models. For comparison with experiment, ω is selected as 25kHz and p_a as $0.13\,p_t$.

From Fig. 4a, the reference length, X_{ref}, is obtained, which is defined as the distance between the subsonic jet exit and the point of 100 m/s local flow velocity (the same as injection velocity, u_2). Then Eq. (6) becomes a closed form. After computation of X_{ref} from a laminar solution, it is converged to a turbulent solution with turbulence models. Fig. 4b visualizes the expansion wave (bright area in numerical shlieren image, plot of the vertical first-order gradient of density) at the expansion edge of rectangular wall and the recompression wave (slightly dark area) before the parallel jet. They are also shown in Ref. [4].

If acoustic waves are impinged into the parallel jet, the transition point is pulled nearer to the nozzle exit, and X_{ref} is shortened in Fig. 4c (see the alternating dark and bright series of acoustic waves). It is evident that the added acoustic wave enhances the mixing of jets. Fig. 4d is solved from Fig. 4c with turbulent models similarly.

The pitot pressure (not total pressure) without supersonic calibration is plotted in Fig. 5a-c. The measuring stations are x/H = 5, 7.5, and 10 (H: the outer height of nozzle, 4 mm), and the pitot pressure is all transformed to a supersonic value using the normal shock relation. The experiment in Ref. [4] and the present computation with turbulence models are well fitted with each other. The mixing is more enhanced if the local minimum pitot pressure is faster recovered to 1.0. The jet width (d) is defined as the 90 %-defect width in the pitot pressure profile as commented in Ref. [4]. The present Navier-Stokes simulation slightly overestimates the mixing width in Fig. 5d but Fig. 5a-d overall validates our method for this investigation very well.

In Fig.1, the self-preserving flow can be observed at a far distance from the nozzle exit. Görtler's similarity solution for two-dimensional free jet and wake are

$$b \sim x \quad \text{for free jet} \tag{8a}$$

$$b \sim x^{1/2} \quad \text{for wake} \tag{8b}$$

and

$$u \sim x^{-1/2} \quad \text{for free jet and wake.} \tag{9}$$

They are compared in Fig. 6a-b with the present numerical simulation of Fig. 4b. The self-similar region is estimated to x/H > 13, and the measuring points of Fig. 5a-c all lie in the developing region. There is recognizable discord between similarity and numerical solutions at the potential core and the developing region due to the nonlinear effects of flow physics.

4. Concluding Remark

A new experimental model for mixing enhancement of parallel supersonic-subsonic mixing jet (M_1=1.78 and M_2=0.30) is simulated with a numerical technique by modeling the wall cavity as an oscillating wall. The oscillating wall is handled with a 'vibrating-wall boundary condition' and emits acoustic waves to disturb the mixing layer of jets.

The obtained pitot pressure distributions along cross sections at the developing region of the turbulent jets are in good agreement with experimental data. The similarity solution of dimensional analysis also coincides with this

numerical result at the self-similar region sufficiently far from the jet exit.

With these results of verification of this method, parametric study will be carried out to find the hidden physics. Parameters may be frequency ($f = w/2p$), amplitude (p_a), and position (X_p in Fig.2).

Fig. 1. A mixing problem of parallel supersonic-subsonic jet.

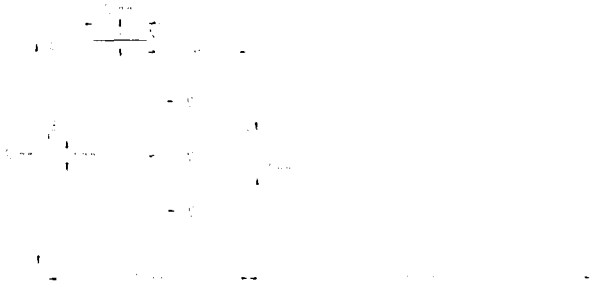

Fig. 2. Problem definition and computational domain.

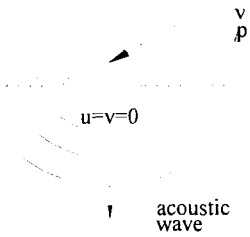

Fig. 3. Vibrating boundary condition.

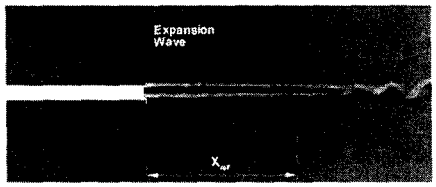

(a) without turbulence model,

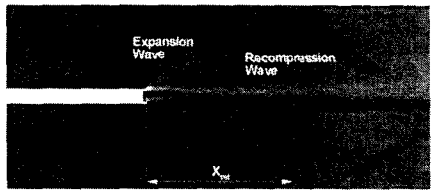

(b)with turbulence model for no wall-vibration

Acknowledgement

This research has been conducted with the financial support of the Korea Science and Engineering Foundation, KOSEF 98-0200-04-01-3 and sponsored by the Brain Korea 21 Project in 2001

References

1. Billig F. S. 1993 Journal of Propulsion and Power 9, 499-514. Research on supersonic combustion.

2. Kumar A., Bushnell D. M. and Hussaini M. Y. 1989 Journal of Propulsion and Power 5, 514-522. Mixing augmentation technique for hypervelocity scramjets.

3. Yu K. H and Schadow K. C. 1994 Combustion and Frame 99, 295-301. Cavity-actuated supersonic mixing and combustion control.

4. Sato N., Imamura S., Shiba S., Takahashi S., Tsue M. and Kono M. 1999 Journal of Propulsion and Power 15, 358-360. Advanced mixing control in supersonic airstream with a wall-mounted cavity.

5. Chang S. M. and Chang K. S. 2000 Shock Waves 10, 333-343. On the shock-vortex interaction in Schardin's problem.

6. Clauser F. H. 1956 Advances in Applied Mechanics 4, 1-51. The turbulent boundary layer.

7. White F. M. 1991 Viscous Fluid Flow (2ed). New York: McGraw-Hill, pp. 470-483.

8. Blackwell B. F. 1973 The turbulent boundary layer on a porous plate: an experimental study of heat transfer behavior with adverse pressure gradients. Ph.D. Thesis, Stanford Univ., California, USA.

9. Chang S. M. and Lee S. 2001 Journal of Sound and Vibration (*in press*). On the jet regurgitant mode of resonant tube.

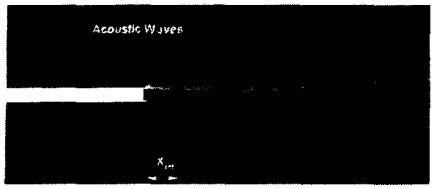

(c)without turbulence model

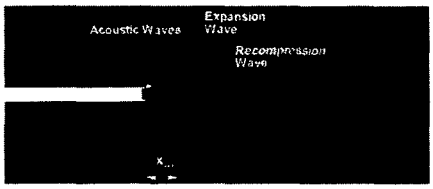

(d)with turbulence model for a wall-vibration case

Fig. 4a-d. Numerical schlieren images:

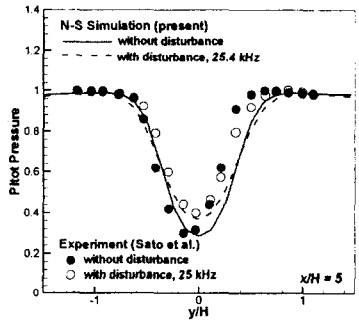

(a) $x/H = 5$

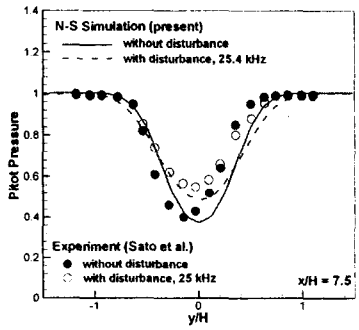

(b) $x/H = 7.5$

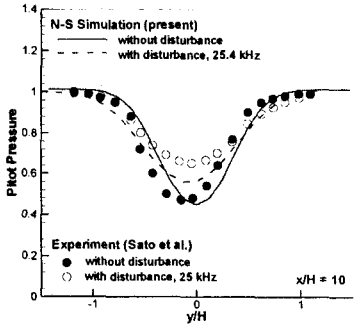

(c) $x/H = 10$

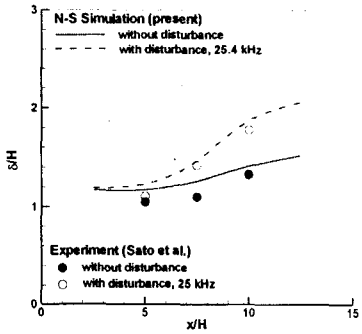

(d) is a plot of jet boundary (d/H) vs. distance from the subsonic jet exit (x/H) along the symmetric axis line ($y = 0$).

Fig. 5a-d. Pitot pressure distribution

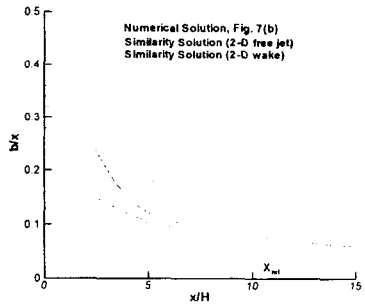

(a)Jet width

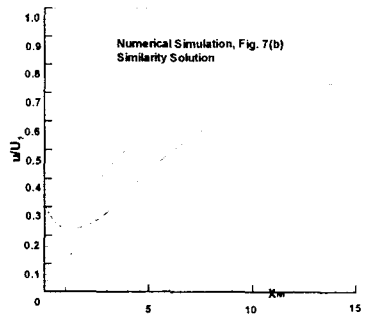

(b)Velocity

Fig. 6a-b. Distributions along the central axis